TU Delft

Delft University of Technology

Document Version
Final published version

Licence
CC BY

Citation (APA)
Morel, J., Baup, F., Fransson, J. E. S., Söderström, M., Parsons, D., Hetta, M., & Steele-Dunne, S. (2026). Time-integrated sentinel-1 backscattering coefficient for monitoring of forage maize development and growth: a pilot study in Sweden. *Acta Agriculturae Scandinavica Section B: Soil and Plant Science* , *76*(1), Article 2713875. https://doi.org/10.1080/09064710.2026.2713875

Important note
To cite this publication, please use the final published version (if applicable).
Please check the document version above.

Copyright
In case the licence states “Dutch Copyright Act (Article 25fa)”, this publication was made available Green Open Access via the TU Delft Institutional Repository pursuant to Dutch Copyright Act (Article 25fa, the Taverne amendment). This provision does not affect copyright ownership.
Unless copyright is transferred by contract or statute, it remains with the copyright holder.

Sharing and reuse
Other than for strictly personal use, it is not permitted to download, forward or distribute the text or part of it, without the consent of the author(s) and/or copyright holder(s), unless the work is under an open content license such as Creative Commons.

Takedown policy
Please contact us and provide details if you believe this document breaches copyrights.
We will remove access to the work immediately and investigate your claim.

This work is downloaded from Delft University of Technology.

Acta Agriculturae Scandinavica, Section B — Soil & Plant Science

ISSN: 0906-4710 (Print) 1651-1913 (Online) Journal homepage: www.tandfonline.com/journals/sagb20

Time-integrated sentinel-1 backscattering coefficient for monitoring of forage maize development and growth: a pilot study in Sweden

Julien Morel, Frédéric Baup, Johan E. S. Fransson, Mats Söderström, David Parsons, Mårten Hetta & Susan Steele-Dunne

To cite this article: Julien Morel, Frédéric Baup, Johan E. S. Fransson, Mats Söderström, David Parsons, Mårten Hetta & Susan Steele-Dunne (2026) Time-integrated sentinel-1 backscattering coefficient for monitoring of forage maize development and growth: a pilot study in Sweden, Acta Agriculturae Scandinavica, Section B — Soil & Plant Science, 76:1, 2713875, DOI: 10.1080/09064710.2026.2713875

To link to this article: https://doi.org/10.1080/09064710.2026.2713875

© 2026 The Author(s). Published by Informa UK Limited, trading as Taylor & Francis Group

Published online: 19 Aug 2026.

Submit your article to this journal

Article views: 220

View related articles

View Crossmark data

Full Terms & Conditions of access and use can be found at
https://www.tandfonline.com/action/journalInformation?journalCode=sagb20

ACTA AGRICULTURAE SCANDINAVICA, SECTION B — SOIL & PLANT SCIENCE
2026, VOL. 76, NO. 1, 2713875
https://doi.org/10.1080/09064710.2026.2713875

Taylor & Francis
by informa

OPEN ACCESS Check for updates

Time-integrated sentinel-1 backscattering coefficient for monitoring of forage maize development and growth: a pilot study in Sweden

Julien Morel [a,b], Frédéric Baup [c], Johan E. S. Fransson [d], Mats Söderström [e], David Parsons [b], Mårten Hetta [f] and Susan Steele-Dunne [g]

[a]European Commission, Joint Research Centre (JRC), Ispra, Italy; [b]Department of Crop Production Ecology, Swedish University of Agricultural Sciences, Umeå, Sweden; [c]Centre d'Etudes Spatiales de la Biosphère, University of Toulouse, CNES/CNRS/IRD/INRAE/UPS, Toulouse, France; [d]Linnaeus University, Department of Forestry and Wood Technology, Växjö, Sweden; [e]Department of Soil and Environment, Swedish University of Agricultural Sciences, Uppsala, Sweden; [f]Department of Applied Animal Science and Welfare, Swedish University of Agricultural Sciences, Umeå, Sweden; [g]Department of Geoscience and Remote Sensing, Delft University of Technology, Delft, the Netherlands

ABSTRACT

The potential of dense Sentinel-2 time series to serve as a basis for operational crop monitoring systems is hindered by cloud cover, especially at high latitudes. Sentinel-1 data can overcome this limitation, but similar to optical data, are prone to saturation, i.e. when changes in vegetation biomass are not reflected in the remote sensing signal. Time-integration is a strategy commonly used in optical remote sensing to mitigate saturation effects. In this pilot study, we tested whether this approach can also improve the relationship between Sentinel-1 backscatter and maize traits, using Sentinel-1 A and B backscatter data. Our test site consisted of a forage maize experimental field in Sweden. Evaluated plant traits included the number of leaves, the phenological stage, the leaf area index, the dry matter yield and the dry matter content. Linear and logistic models were adjusted between time-integrated values of the backscattering coefficient (σ^0_{VH}, σ^0_{VV}, $\sigma^0_{VH\times VV}$ and $\sigma^0_{VH/VV}$) and field-measured traits. Our results indicate a good agreement between Sentinel-1 time-integrated signal and maize traits, with R^2 of 0.97, 0.93, 0.94, 0.95 and 0.86 for phenological stage, leaf number, leaf area index, dry matter yield and dry matter content, respectively, and systematically outperformed models built with non-cumulative σ^0 values. Our findings also indicate that the time-integrated models perform equally well with data acquired from a single Sentinel-1 satellite. These results, if confirmed for a wider range of geographical extent and management conditions, could pave the way for a remote sensing-based, weather-independent and saturation-insensitive decision support tool.

ARTICLE HISTORY
Received 31 March 2026
Accepted 31 July 2026

KEYWORDS
Cumulative backscattering coefficient; maize monitoring; Sentinel-1

Introduction

Earth Observation satellites have become a major tool for food security and policy support through large-scale monitoring of agricultural and ecological systems (Fritz et al. 2019). In operational research, satellite data are used for various agricultural-related objectives, for example crop type mapping, phenology tracking, yield estimation, evaluation of fertilisation requirements, etc., as summarised in Bégué et al. (2018) and Weiss et al. (2020). A growing number of satellites with higher spatial resolution allows for increasingly dense time series of radiometric data that capture dynamics of vegetation from field to continental scales (Belward and Skøien 2015; Gómez et al. 2016). In particular, the launch of the Sentinel-1 and Sentinel-2 constellations was a major milestone for the acquisition of time-dense, high-spatial resolution, open-access microwave and optical data, respectively (Veloso et al. 2017).

Most agricultural-related remote sensing studies report the use of optical data, as illustrated in Figure 1 – the number of publications using Sentinel-2 data has been greater than those using Sentinel-1 data. The most obvious reason for this is that optical data are easier to interpret and link to vegetation properties such as pigments or leaf area index compared to microwaves, considering the multiple contributions of

CONTACT Julien Morel julien.morel@slu.se Swedish University of Agricultural Sciences, Skogsmarksgränd 17 Umeå 901 83, Sweden

© 2026 The Author(s). Published by Informa UK Limited, trading as Taylor & Francis Group
This is an Open Access article distributed under the terms of the Creative Commons Attribution License (http://creativecommons.org/licenses/by/4.0/), which permits unrestricted use, distribution, and reproduction in any medium, provided the original work is properly cited. The terms on which this article has been published allow the posting of the Accepted Manuscript in a repository by the author(s) or with their consent.

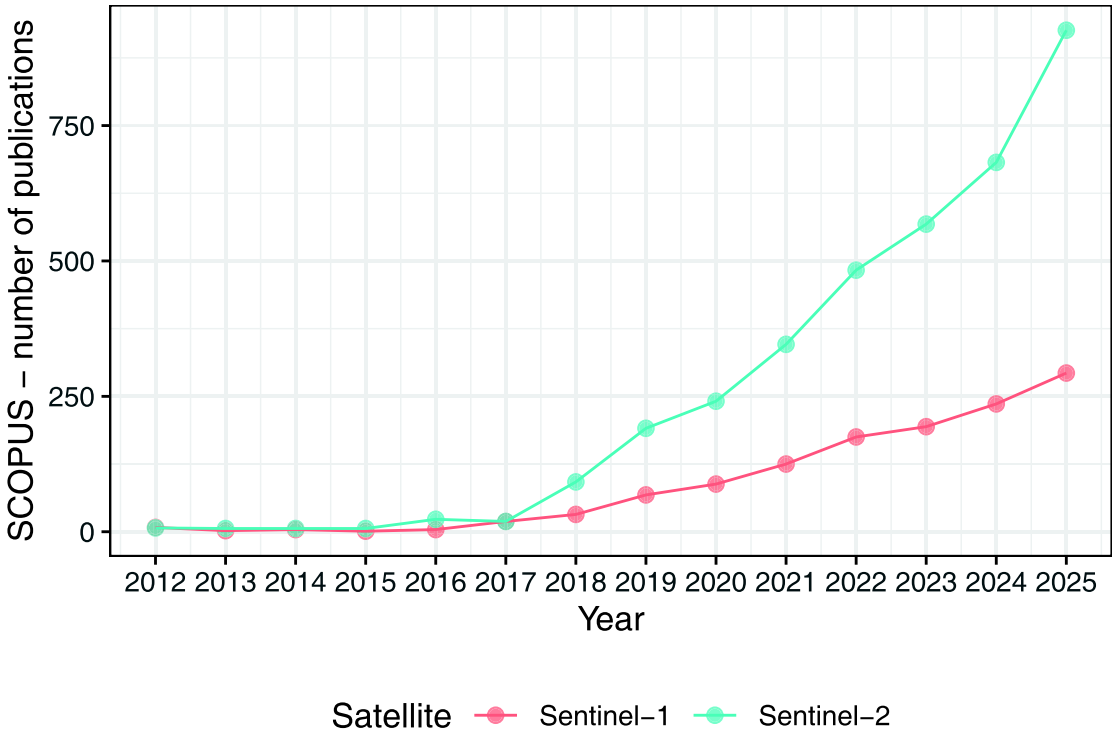

Figure 1. SCOPUS search results for publications that contain 'Sentinel-1' or 'Sentinel-2' in their title, abstract or keywords (subject area: Agricultural and Biological Sciences). Accessed on 2026-03-04.

vegetation, soil, and interactions between soil and vegetation in a microwave backscattering coefficient (Steele-Dunne et al. 2017). Nevertheless, converting optical sensor data into operational decision support tools is limited by cloud cover, which affects the availability and reliability of spectral information (Weiss et al. 2020; Kooistra et al. 2024). In contrast, microwave satellites such as Sentinel-1 using active sensors offer advantages, as long wavelengths ensure observation availability regardless of cloud cover.

As a prerequisite to operational applications, Veloso et al. (2017) interpreted time series of backscattering coefficients for six major crops (wheat, barley and rapeseed for winter crops, and soybean, sunflower and maize for summer crops) in south-western France. They reported that the cross-polarisation ratio ($\sigma^0_{VH/VV}$) acquired from Sentinel-1 SAR is strongly linked to the growth cycle, as it minimises the ground contribution while maximising the vegetation signal, making it a promising proxy to track biomass accumulation of crops. Building on these findings, recent multi-annual analyses demonstrated that combined SAR and optical satellite time series can be consistently modelled using parametric approaches such as double logistic functions, enabling robust characterisation of crop phenology and interannual variations driven by climatic conditions and agricultural practices (Baup et al. 2026). Similarly, Khabbazan et al. monitored sugar beet, potato, maize, wheat and English ryegrass over the agricultural area of Flevopolder in The Netherlands with time series of σ^0 and interferometric coherence data (Khabbazan et al. 2019). They concluded that σ^0 dynamics are related to changes in water content and structure of the crop associated with phenological development, and that sharp changes in interferometric coherence can be used for harvest detection.

Several studies have confirmed the potential of Sentinel-1 satellite data for crop monitoring. For example, it has been successfully used with artificial intelligence to perform field crop type mapping at regional (Di Martino et al. 2022; Planque et al. 2021) and continental (d'Andrimont et al. 2021) scales. Similarly, phenology dynamics of various crops were retrieved from Sentinel-1 backscattering coefficient at regional scale (d'Andrimont et al. 2020; Qadir et al. 2023), or over Europe (Meroni et al. 2021). Crop productivity indicators were assessed, such as, for example, sucrose content of sugarcane (den Besten et al. 2023) or dry matter of wheat, soybean and canola (Mandal et al. 2020). Variables of importance for water management have also been explored, such as soil moisture content (Quast et al. 2023; Schmidt et al. 2024), irrigation (Bazzi et al. 2020), waterlogging (den Besten et al. 2023) or drought (Shorachi et al. 2022).

However, similar to optical remote sensing, C-band backscattering coefficient is prone to saturation at high levels of biomass, as reported in Mandal et al. (2020), Allies et al. (2021), Ameline et al. (2018) and Wiseman et al. (2014). Although both optical and SAR signals saturate at high biomass, the mechanisms differ. Optical saturation is caused by the fact that reflectance is predominantly a surface (canopy) phenomenon, which reaches an asymptote when canopy is closing. SAR backscatter, in contrast, results from a mixture of soil surface, canopy volume, and surface-volume interaction scattering, with the volume component becoming increasingly dominant as the canopy develops. Because C-band's penetration into dense canopies is limited, the recorded signal increasingly reflects only the upper canopy layers; beyond a certain biomass and water content, volume scattering plateaus and the signal becomes insensitive to further biomass increases.

In optical remote sensing, one solution to overcome this issue is to integrate the signal over time (i.e. compute the cumulative sum of the signal from a defined start date, such as sowing, onward), as done, for example, with the seasonal integral of the normalised difference vegetation index (NDVI). This has been reported to perform well for agricultural monitoring purposes such as above-ground biomass estimation or phenology metrics, either as a stand-alone (Campoy et al. 2023; Shammi and Meng 2021) or combined with meteorological data in a simple crop model (Claverie et al. 2012; Morel et al. 2014; Battude et al. 2016; Baup et al. 2019). This approach has the advantage of being easy to implement and integrates the seasonal photosynthetic activity (Hird and McDermid 2009), but, in the case of optical sensors, is still limited by the cloud cover. This can, therefore, hamper the smoothing and interpolation processes required to integrate signal over time.

Cloud cover does not limit Sentinel-1 data acquisition, and promising results have recently been shown with time-integrated Sentinel-1 signals for wheat (Gorrab et al. 2021) and rapeseed (Allies et al. 2021). Maize, however, presents particular challenges for SAR-based crop monitoring compared with many other agricultural crops. Its rapid development produces a tall and dense canopy with large leaves and thick stems, resulting in complex scattering mechanisms involving soil, vegetation volume and double-bounce interactions. As biomass increases, the C-band Sentinel-1 backscatter progressively saturates, reducing its sensitivity to additional crop growth during the reproductive stages (Wiseman et al. 2014; Ameline et al. 2018; Mandal et al. 2020; Allies et al. 2021). Furthermore, instantaneous backscatter measurements are strongly influenced by rainfall events, soil moisture variations and changes in plant water content, making the relationship between SAR observations and maize biophysical variables highly variable throughout the growing season. These limitations have constrained the operational use of Sentinel-1 for monitoring high-biomass crops such as maize using conventional image-by-image approaches.

In this study, we hypothesise that integrating Sentinel-1 backscatter over time can overcome these limitations. By accumulating the radar signal from sowing to harvest, the proposed approach emphasises the cumulative structural development of the crop while reducing the influence of short-term fluctuations caused by weather conditions and soil moisture. We therefore investigate whether time-integrated Sentinel-1 backscatter provides a more robust indicator of maize phenology and growth than conventional instantaneous SAR observations.

The aim of this pilot study was to explore the performances of cumulative (i.e. time-integrated) backscattering coefficient signals to monitor the growth and development of experimental maize fields in southern Sweden. Simple univariate regression models (linear- and logistic-based) were used, as they are computationally inexpensive and easier to conceptualise, manipulate and transfer compared to non-linear machine learning algorithms, such as random forest and support vector machines.

Materials and methods

Field data

Field data were collected in 2021 at the experimental farm of the Swedish Rural Economy and Agricultural Societies (*Hushållningssällskapet*) in Skåne in southern Sweden (56.0°N, 14.1°E). The field experiment consisted of four quadrants with 120 m sides, located on a sandy soil (Figure 2). The terrain is flat, reducing potential geometry effects on the backscatter signal (Veloso et al. 2017). Four maize cultivars were selected to encompass a range of phenological development rates using FAO numbers (Zscheischler et al. 1990)

Figure 2. Layout of the field experiment located in southern Sweden (red area in the inset map of Sweden). Each cultivar was sown in a 120 m × 120 m quadrant, divided into nine sampling areas of 40 m × 40 m that were used for each sampling event.

typical of what is used for silage maize in Sweden. A unique cultivar (cv.) was used for each quadrant: Autens cv. (FAO 170), Kompetens cv. (FAO 180), Megusto cv. (FAO 200) and Stefano cv. (FAO 210).

Maize was sown on the 14th of May 2021. Each quadrant was divided into nine sampling areas that were used in a random order to perform field measurements, destructive harvests and laboratory measurements. Ground data acquisition started on the 29th of June 2021 and ended on the 15th of September 2021, and consisted of nine sampling dates. For each sampling area and sampling date, three randomly selected 2 m-long lines were used for field measurements. Field-measured plant traits included phenology, expressed in BBCH (*Biologische Bundesanstalt, Bundessortenamt und CHemische Industrie*) scale, as presented by Lancashire et al. (1991), and the number of green leaves. Leaf area index (LAI, expressed in $m^2 \cdot m^{-2}$), dry matter content (DMC, expressed in $g \cdot kg^{-1}$) and dry matter yield (DMY, expressed in $t \cdot ha^{-1}$) were determined by destructive sampling. In a laboratory, plants were separated into fresh leaves, stems and cobs. The leaf area was measured using a WinDIAS Leaf Image Analysis System (Delta-T Devices Ltd, England). LAI was calculated based on the measured green leaf area with a sample length of 2 m and row spacing of 0.75 m. Leaves, stems and cobs were then placed in a drying cabinet at 60°C for 48 hours (or until constant weight was reached) to measure their dry weight and compute their DMC (i.e. the ratio of dry mass to the fresh

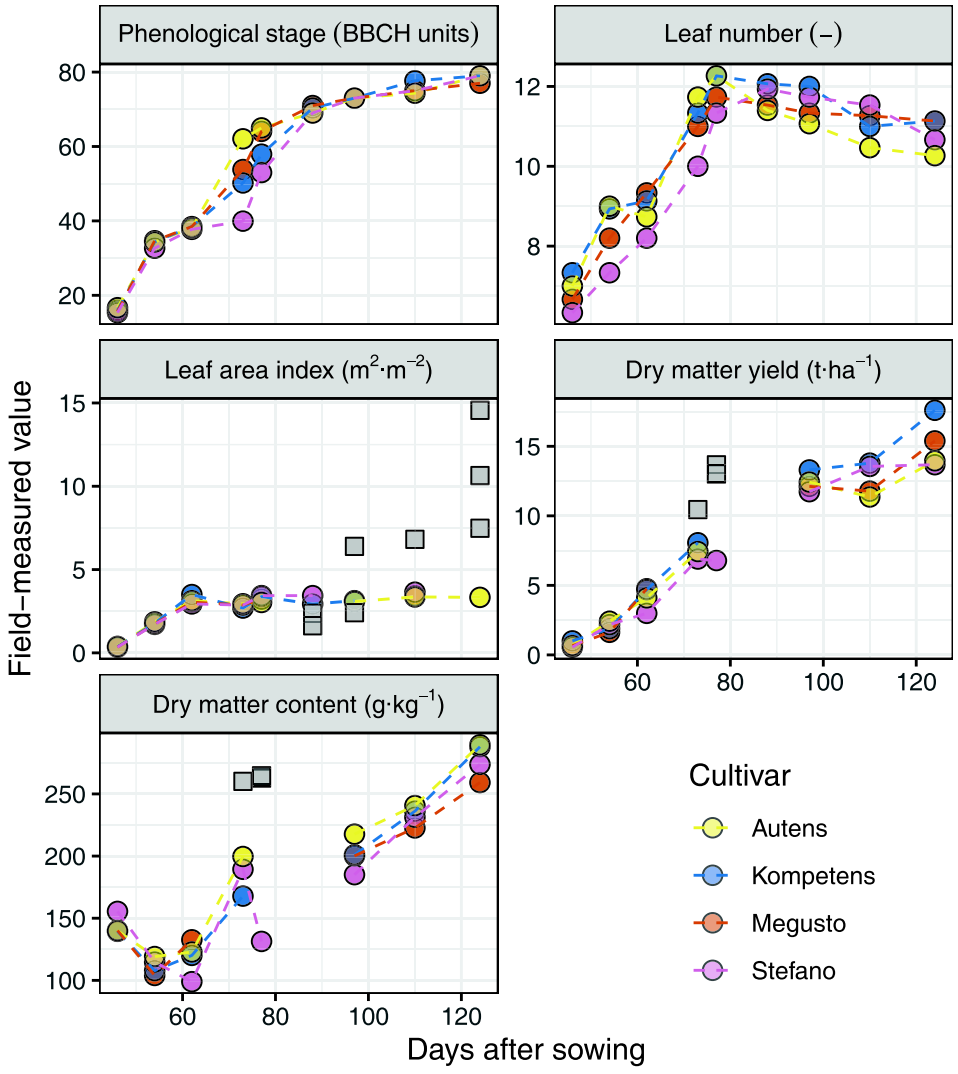

Figure 3. Field measurements for each cultivar. Grey squares indicate measurements that were discarded from analysis (see main text).

mass, which is a key indicator to determine the optimal harvest window for silage maize). DMY was computed from the dry weight (including stems, leaves and cobs), sample length and row spacing. A total of 36 ground truth datapoints were available for each plant trait (nine sampling dates for the four quadrants, Figure 3).

However, due to measurements issues for DMC and leaf area, some samples for LAI, DMY and DMC were filtered out based on expert knowledge – i.e.assessment by the agronomic researchers and field-trial managers involved in data collection, informed by expected physiological behaviour of silage maize reported in the literature – to minimise the risk of introducing noise in our models (grey squares in Figure 3). Indeed, for silage maize, DMY and DMC are expected to increase consistently throughout the growth phase under optimal growing conditions (Hetta et al. 2012), while maximum LAI values typically range between 3 and 6 (Kalogeropoulos et al. 2024). LAI measurements for cv. Megusto at 88 and 97 days after sowing (DAS) and cv. Autens at 88 DAS were discarded because they were out of the range of measurement uncertainty – it is unclear what was the source of these errors. The DMC values for cv. Stefano collected on 26th and 30th July (DAS 73 and 77 in Figure 3) were retained for analysis because the cause of the apparent outliers could not be determined and day-to-day variation in DMC can occur in response to environmental conditions. Hence, 36 measurements were available for BBCH and leaf number, and 28 were available for LAI, DMY and DMC.

Sentinel-1 data

The Sentinel-1 constellation, equipped with synthetic aperture radar (SAR) instruments, is managed by the European Space Agency (ESA) as part of the Copernicus programme. Sentinel-1 data are acquired in the C-band (6 cm-long wavelengths), which makes the signal insensitive to cloud cover. Data for a given area can be collected from different passes (i.e. ascending or descending) and orbits (in this case numbers 73, 95, 146 and 168), which increases the revisit frequency, but also results in different azimuth and range directions that need to be considered when analysing the radar data (Table 1). For a more comprehensive description of the satellites and their payloads, the reader is referred to Torres et al. (2012).

Image products in ground range detected (GRD) format, with incidence angles ranging from 35° to 43°, were pre-processed using Google Earth Engine (Gorelick et al. 2017). Figure 4 summarises the workflow, which included a radiometric calibration, thermal noise removal and terrain correction, similar to what was proposed in Baup et al. (2019). Note that the average signal is considered for each plot. Therefore, applying speckle filtering is unnecessary, as one of its properties is to preserve the average at the scale of a segmented unit, such as an agricultural field.

The images were resampled to a pixel size of 10 m × 10 m corresponding approximately to the spatial resolution. Values for the backscattering coefficient signals (σ^0_{VH}, σ^0_{VV}, $\sigma^0_{VH\times VV}$ and $\sigma^0_{VH/VV}$), expressed in dB, were then averaged over each quadrant (120 m × 120 m), the size of which was designed to minimise the speckle effect inherent to SAR data. $\sigma^0_{VH\times VV}$ and $\sigma^0_{VH/VV}$ were computed as follows:

$$\sigma^0_{VH\times VV} = \sigma^0_{VH} + \sigma^0_{VV} \tag{1}$$

$$\sigma^0_{VH/VV} = \sigma^0_{VH} - \sigma^0_{VV} \tag{2}$$

A total of 213 images were acquired during 2021, with 92 images available between the sowing and the harvest of the maize fields, corresponding to approximately one image every 1.5 days (Figure 5). As a comparison, during the same period, 25 Sentinel-2 images were acquired over the monitored fields, of which only two were cloud free. The time series of $\sigma^0_{VH\times VV}$ values before sowing shows a baseline around −40 dB, yet large variations are reported. In particular, high backscattering coefficient values (i.e. greater than −25 dB) can be related to identified rainfall events. The signal then shows a clear increasing pattern starting shortly after sowing and ending in early July (Figure 5), followed by a plateau related to the saturation effect. Finally, a progressive decrease of $\sigma^0_{VH\times VV}$ from harvest onward can be observed. This was previously reported by Veloso et al. (2017), who explained that such a decrease is related to standing green residues that progressively dry out. This decrease, in our case, might have been counterbalanced by the heavy rainfall that was reported after harvest (Figure 5), which is expected to increase the backscattering coefficient.

Regression models

Regression models were fitted for phenological stage (BBCH), leaf number, LAI, DMY and DMC using time-integrated values of backscattering coefficients, i.e. $\Sigma\sigma^0_{VH}$, $\Sigma\sigma^0_{VV}$, $\Sigma\sigma^0_{VH\times VV}$ and $\Sigma\sigma^0_{VH/VV}$, as explanatory variables. The starting point for time integration was set on the sowing date (i.e. the 14th of May 2021) and ended on the harvest date (i.e. the 5th of October 2021).

Three types of time integrations were performed. First, with every available Sentinel-1 image being used (i.e. mixing information from the different orbits, hereinafter referred to as a mixed orbit signal). Then, time integration was performed separately for each orbit, hereinafter referred to as a single orbit signal. In the

Table 1. Sentinel-1 data available over the study area.

Relative orbit	Pass	Local time	Median incidence angle (°)	Number of images
73	Ascending	16:45	35.6	56
95	Descending	05:15	42.8	43
146	Ascending	16:53	43.1	58
168	Descending	05:24	35.3	56

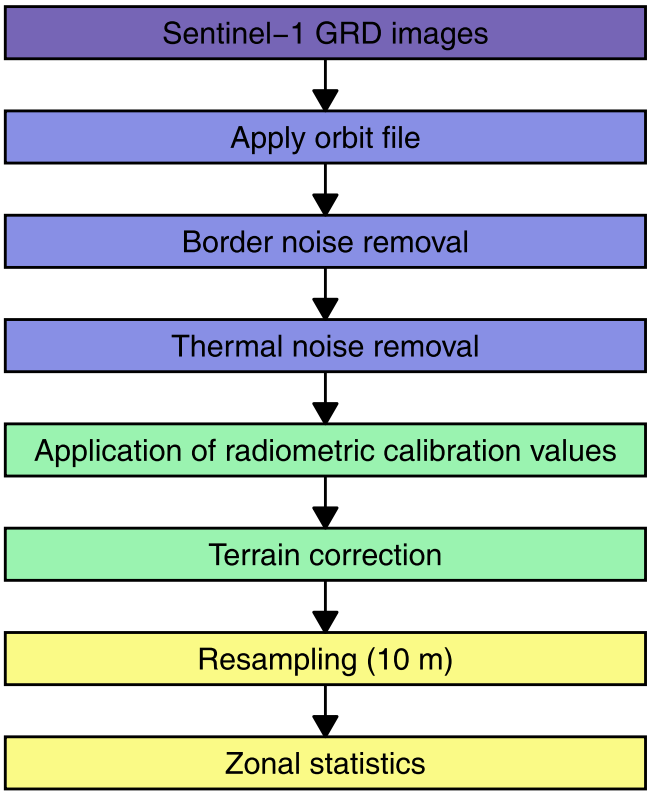

Figure 4. Flowchart of the preprocessing of the Sentinel-1 data.

latter case, some field measurements could not be matched against a satellite observation for the same date. Two approaches were therefore tested to overcome this issue: (i) using the cumulated value of the closest satellite observation and (ii) deriving a cumulative value from a linear interpolation using the closest pre- and post-field measurement for the satellite observations.

Using these cumulative values, two types of models were used, namely linear and logistic regression, depending on the relationship between the cumulative backscattering coefficient and the trait of interest.

Linear regressions were developed using the following generic equation:

$$y = a \cdot x + b + \epsilon \tag{3}$$

where y is the response variable (i.e. BBCH, leaf number, LAI, DMY and DMC), x is $\Sigma\sigma^0$, a and b the slope and intercept, respectively, and ε is the residual error.

Logistic regressions were developed using the following generic equation:

$$y = \frac{m}{\left(1 + e^{-c(x - x_i)}\right)} + \epsilon \tag{4}$$

where m is the maximum $\Sigma\sigma^0$ of the logistic curve, c is the slope at the inflection point of the function, and x_i is $\Sigma\sigma^0$ at the inflection point i.

Regression models were built using both (i) the full dataset and (ii) a leave-one-out cross validation to ensure that our models did not overfit, while maximising the use of our dataset. Finally, for the sake of comparison, models were also built using a non-integrated backscattering coefficient, using the full dataset, and linear regressions as described in Equation (3). Model performance was evaluated using two metrics: the coefficient of determination (R^2) and the root mean square error (*RMSE*).

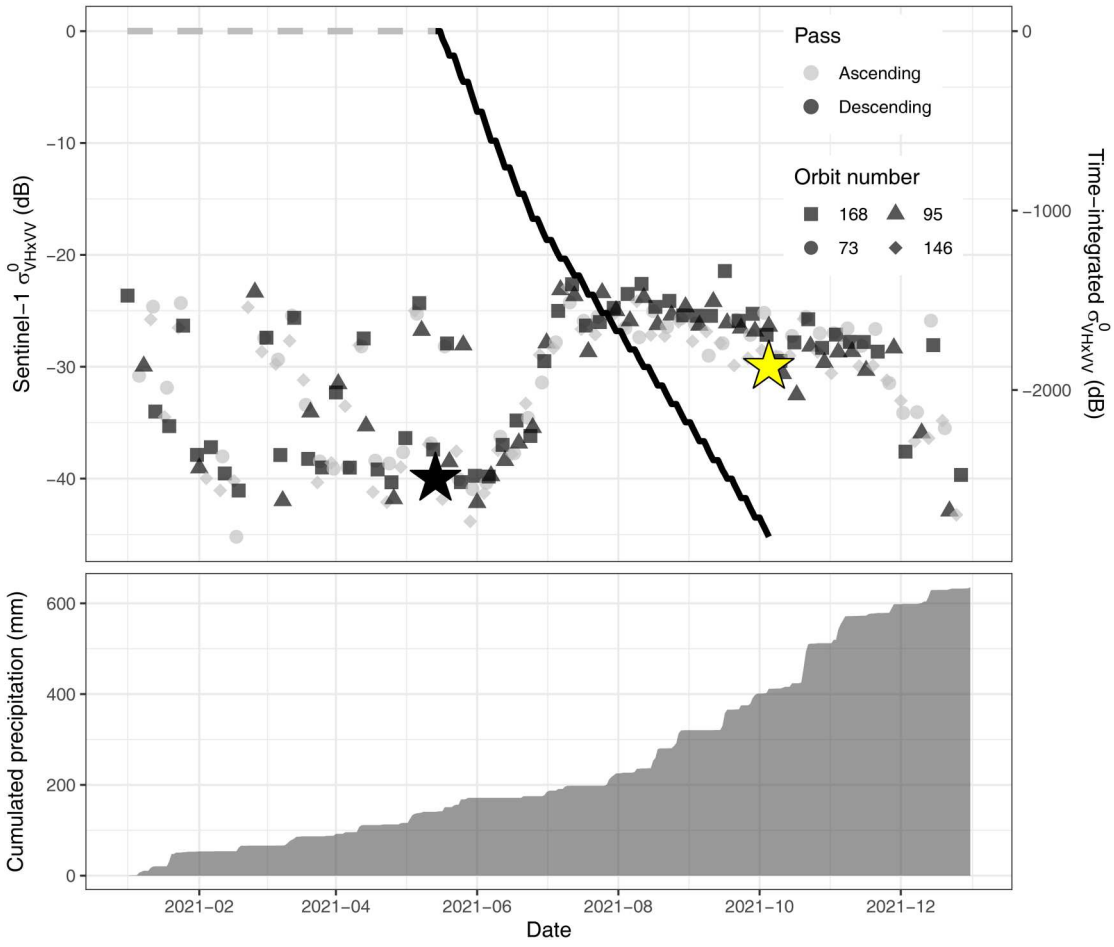

Figure 5. Time series of $\sigma^0_{VH\times VV}$ and rainfall events obtained for the Autens cultivar. Symbols show daily values and the black line shows the time-integrated values. The black star indicates sowing and the yellow star indicates harvest (upper panel).

Results and discussion

Evaluation of development and growth indicators of forage maize

Results presented in this section, unless stated otherwise, refer to models built using the mixed orbit signal (i.e. with a cumulative signal computed using Sentinel-1 images from all orbits), using the complete dataset, as no notable difference was reported when using the leave-one-out cross validation (Appendix 1).

All regression models fitted for the development and growth traits assessed in the study showed strong accuracy, with the best models achieving R^2 values ranging between 0.86 and 0.97 (Table 2). Regression coefficients are provided in Table A1 (Appendix 2).

A clear non-linear trend was observed between $\Sigma\sigma^0$ and phenology (Figure 6(a)). A logistic regression was applied to account for this non-linearity. Best results were obtained with $\Sigma\sigma^0_{VH\times VV}$, with an R^2 of 0.97 and an *RMSE* of about 4 BBCH units (Table 2, Figure 6(b)). Field measurements performed on days after sowing (DAS) 73 and 77 show large variability in BBCH compared to other sampling dates. This variability is most probably related to the fact that measurements were performed during the inflorescence and flowering stages (BBCH units ranging from 51 to 69), during which a precise BBCH estimation can be difficult to obtain. This can introduce variability in the BBCH values depending on the field operator that performed the measurements.

The evolution of the number of green leaves in time showed two clear patterns: one steep increase from sowing until 77 DAS, followed by a steady decrease until harvest (Figure 6(c)). This shift corresponds to a transition from the vegetative phase (during which stem and leaf biomass increase), to the reproductive phase (when the products of photosynthesis are mostly allocated to grains) and leaf senescence. Therefore,

Table 2. Statistical indicators of performances of regression models in terms of *RMSE* and R^2.

Variable	$\Sigma\sigma^0$	Model type	*RMSE*	R^2
BBCH	σ^0_{VH}	Logistic	3.80	0.97
BBCH	$\sigma^0_{VH/VV}$	Logistic	4.77	0.95
BBCH	$\boldsymbol{\sigma^0_{VH\times VV}}$	**Logistic**	**3.77**	**0.97**
BBCH	σ^0_{VV}	Logistic	3.85	0.97
Leaf number	σ^0_{VH}	Linear*	0.47	0.93
Leaf number	$\boldsymbol{\sigma^0_{VH/VV}}$	Linear*	0.56	0.90
Leaf number	$\boldsymbol{\sigma^0_{VH\times VV}}$	**Linear***	**0.46**	**0.93**
Leaf number	σ^0_{VV}	Linear*	0.46	0.93
LAI	$\boldsymbol{\sigma^0_{VH}}$	**Logistic**	**0.26**	**0.94**
LAI	$\sigma^0_{VH/VV}$	Logistic	0.31	0.92
LAI	$\sigma^0_{VH\times VV}$	Logistic	0.29	0.93
LAI	σ^0_{VV}	Logistic	0.33	0.90
DMY	σ^0_{VH}	Linear	1.23	0.95
DMY	$\sigma^0_{VH/VV}$	Linear	1.45	0.93
DMY	$\boldsymbol{\sigma^0_{VH\times VV}}$	**Linear**	**1.21**	**0.95**
DMY	σ^0_{VV}	Linear	1.22	0.95
DMC	σ^0_{VH}	Linear	2.32	0.85
DMC	$\sigma^0_{VH/VV}$	Linear	2.52	0.83
DMC	$\sigma^0_{VH\times VV}$	Linear	2.29	0.86
DMC	$\boldsymbol{\sigma^0_{VV}}$	**Linear**	**2.26**	**0.86**

Notes: BBCH refers to the phenological stage, LAI stands for leaf area index, DMY stands for dry matter yield and DMC stands for dry matter content. Bold characters indicate the signal with best performances for each variable. Linear* denotes a double linear regression to account for the shift from the vegetative phase to the reproductive phase and is further detailed in the main text.

a piece-wise linear model was developed to account for this, i.e. one for the vegetative phase and one for the reproductive. To this end, a threshold was set to phenological stage 61 BBCH units, corresponding to the start of maize flowering, and marking the switch from the vegetative to the reproductive phase. Best performances were obtained with $\Sigma\sigma^0_{VH\times VV}$, with an R^2 of 0.93 and an *RMSE* of about 0.5 (Table 2, Figure 6(d)).

Similar to the BBCH stage, a strong non-linear relationship was observed between the LAI and the time-integrated backscattering coefficient (Figure 7(a)). A logistic regression was fitted to account for this non-linearity. The best results were obtained with $\Sigma\sigma^0{}_{VH}$, with an R^2 of 0.94 and an *RMSE* of about 0.3 (Table 2, Figure 7(b)). It is also worth noting that measurements taken on 73 DAS show a slight decrease of LAI, which is most likely related to a field measurement issue, introducing some noise and reducing the overall performance of the model.

A linear regression was built to link the DMY with the time-integrated backscattering coefficient (Figure 7(c)). Best results were obtained with $\Sigma\sigma^0_{VH\times VV}$ signal, with an R^2 of 0.95 and an *RMSE* of 1.2 $\mathrm{t}\cdot\mathrm{ha}^{-1}$ (Table 2, Figure 7(d)).

A linear regression model was fitted between the DMC and the backscattering coefficient (Figure 7(e)). Best results were obtained with $\Sigma\sigma^0_{VV}$. This is consistent with expectations, as it has been reported that this polarisation configuration is the most sensitive to variations of plant moisture content (Baup et al. 2019). The model showed good performances, with an R^2 of 0.86 and an *RMSE* of about 2.3 $\mathrm{g}\cdot\mathrm{kg}^{-1}$ (Table 2, Figure 7(f)). In the early stages of development of the maize plant (46 to 62 DAS), the amount of biomass is low while the water content is high as the plant material mostly consists of young leaves. Therefore, the error in determining the DMC in these stages is larger compared to the other stages, and the natural variation of the DMC is higher.

This explains the large variation of DMC in early sampling instances. The DMC is a key indicator to determine the optimal harvest window for forage maize, and should increase to a value of around 330 $\mathrm{g}\cdot\mathrm{kg}^{-1}$ (Hetta et al. 2012). The *RMSE* value reported for DMC (Table 2) corresponds to a mean normalised error of estimation of approximately 12%, which could be considered too high for practical applications. However, the performances of the model are likely underestimated, as we included noise in our regression with measurements performed for Stefano cv. collected on 73 and 77 DAS, as reported in Subsection 'Field data'. Moreover, a model intended for practical applications should deliver superior performance for DMC values above 250 $\mathrm{g}\cdot\mathrm{kg}^{-1}$: while our model performs reasonably well for both low and high DMC values, its performance is likely to improve in an operational context.

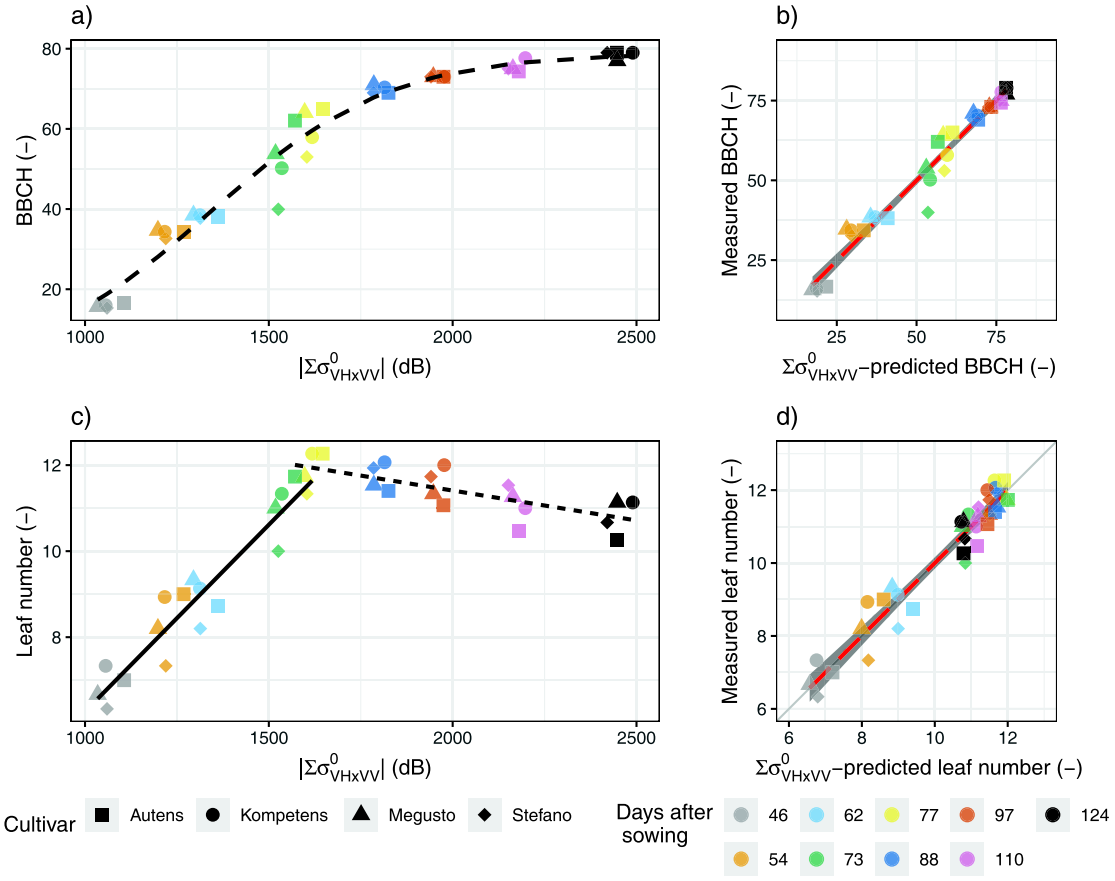

Figure 6. Relationships between $\Sigma\sigma^0_{VH\times VV}$ and phenological stage (BBCH) and leaf number (plots a and c), where black lines indicate the regression line. Note that for the leaf number, a piece-wise linear regression was adjusted, resulting in two black lines (full and dashed) in plot c. Plots b and d show corresponding linear regression models where shaded areas indicate the 95% confidence interval, red dashed lines indicate the regression line and grey lines indicate the 1:1 line. Note that for the sake of readability, absolute values of time-integrated backscattering coefficient are used (plots a and c).

To the best of our knowledge, no previous study has been published on the use of time-integrated backscattering coefficients for maize. However, our results are similar to those obtained for rapeseed in Allies et al. (2021), where models built using the cumulative sums of Sentinel-1 σ^0 reported good matches against field-measured plant height (R^2 of 0.87), water content (R^2 of 0.76), and fresh (R^2 of 0.73) and dry mass (R^2 of 0.82). Gorrab et al. (2021) compared temporal profiles of several Sentinel-1 backscattering coefficient combinations with field measured fresh mass, dry mass, plant height and water content of wheat fields in southwestern France. They reported that time-integrated backscattering coefficients had R^2 of 0.6 for water content, 0.75 for fresh mass and 0.9 for dry mass and plant height, and that $\Sigma\sigma^0$ systematically outperformed non-cumulative backscatter in terms of explained variability. Our results support these findings, while also indicating that the time-integrated backscatter approach is also suitable for dense canopy and high biomass crops such as maize (shown here) and potentially sugarcane.

Effects of the incidence angle

Higher incidence angles (i.e. >35°) increase the path length through vegetation, maximising the contribution of vegetation in the signal (Veloso et al. 2017), which should result in higher accuracy models compared to steeper incidence angles. However, in this study, time integration of the backscatter signal using single orbits (i.e. angles) did not show noticeable differences. Similarly, models built on single orbit signal and models for which time integration was done using signals from all orbits (i.e. mixed orbits) showed similar accuracies (Figure 8).

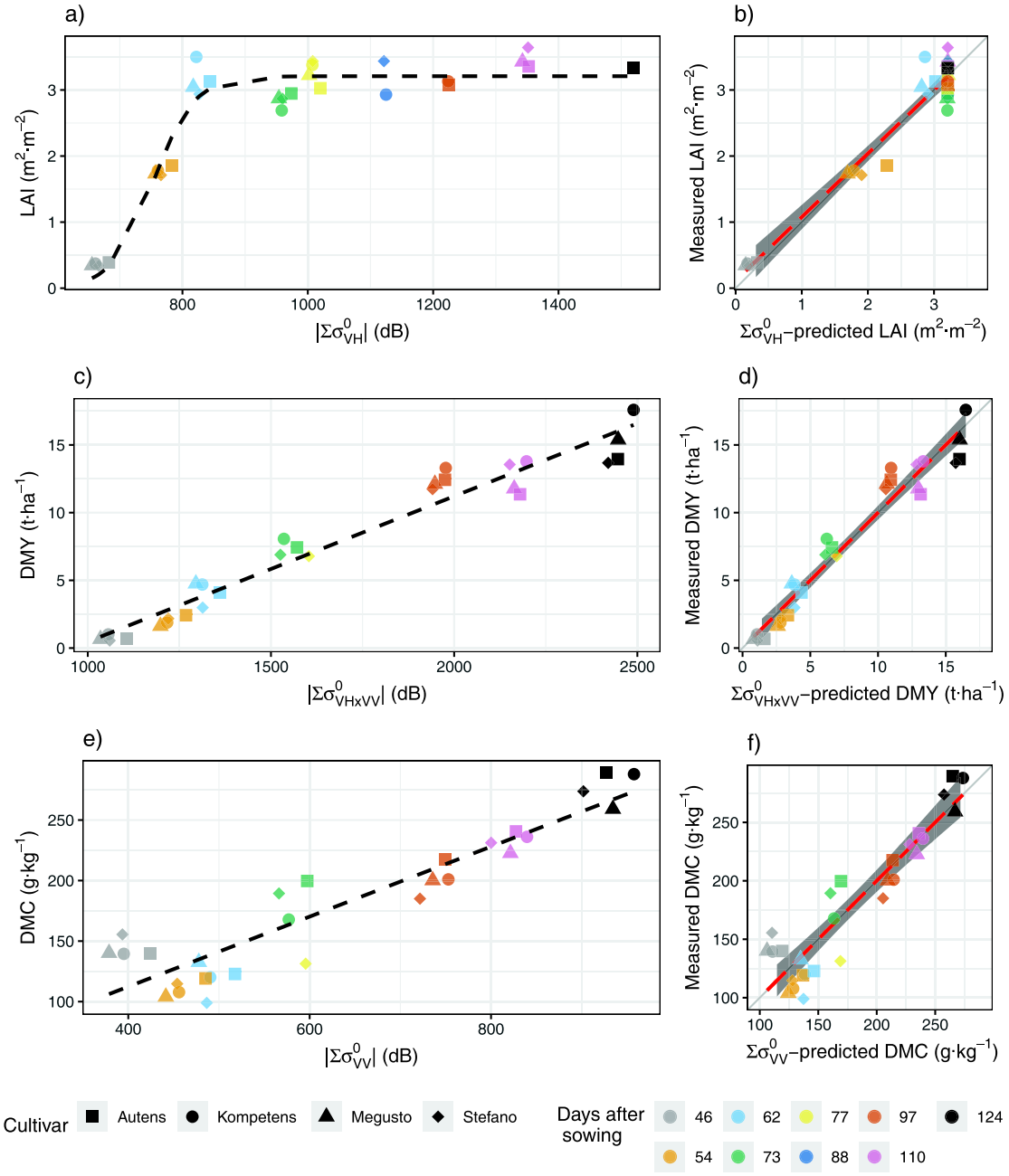

Figure 7. Relationships between $\Sigma\sigma^0$ and leaf area index (LAI), dry matter yield (DMY) and dry matter content (DMC) (plots a, c and e), where black dashed lines indicate the regression line. Plots b, d and f show corresponding linear regression models, where shaded areas indicate the 95% confidence interval, red dashed lines indicate the regression line and grey lines indicate the 1:1 line. Note that for the sake of readability, absolute values of time-integrated backscattering coefficient are used (plots a, c and e).

Influence of the revisit frequency

Following a power supply anomaly on the 23rd of December 2021, the Sentinel-1 B mission ended prematurely. While this did not affect our data acquisition, the loss of Sentinel-1 B resulted in a significant reduction of the revisit frequency that could have compromised the accuracy of the results presented in this study. However, as Figure 8 shows, single orbit-based models were similar in accuracy compared to mixed orbit models, despite significantly different acquisition frequencies during the growth period: 1.5 days for mixed orbit models, compared to 6 days for orbits 73, 146 and 168, and 12 days for orbit 95. This suggests that the loss of a Sentinel-1 satellite would not affect the performances of the time-integrated models.

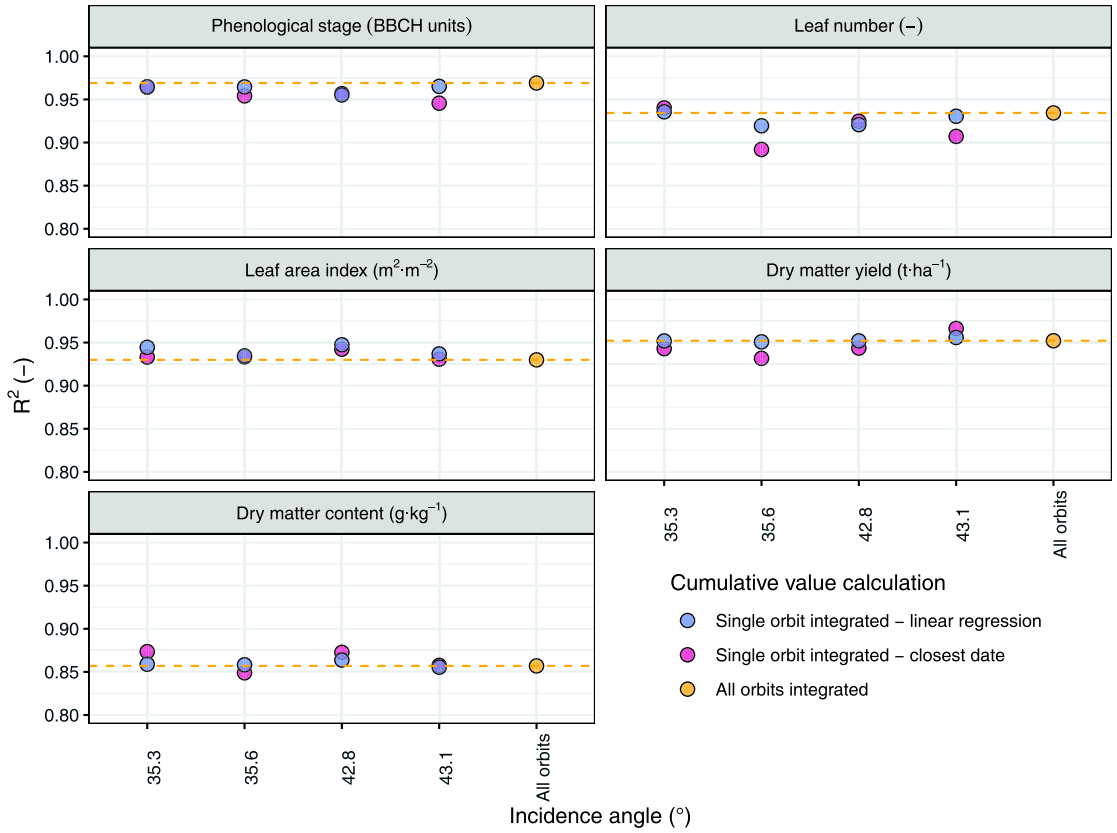

Figure 8. Effects of orbit incidence angles on R^2 for each variable, obtained from $\sigma^0_{VH\times VV}$. The dashed orange lines show values obtained when integrating all orbits.

Comparison with non-integrated backscattering coefficient

Non-integrated σ^0-based regression models systematically showed lower performances compared to $\Sigma\sigma^0$-based models (Table 3).

These performance differences are most likely linked to the saturation effect reported in Allies et al. (2021), Mandal et al. (2020), and Wiseman et al. (2014), but also to the fact that integrating the signal through time reduces the influence of rapid surface changes (rainfall, wind gusts, tillage events, etc.) on the backscattering coefficient.

Considerations for transferability toward an operational system

Maize is a major crop worldwide, and our approach could address operational needs for both farmers and policy-makers. At the farm level, monitoring of the dry matter content and dry matter yield could help farmers make informed decisions about the optimal harvest date. On a larger scale, such a tool could be applied to estimate maize production at regional or national level, which is important information for policy-makers.

Table 3. Coefficients of determination (R^2) for different variables and signals.

Variable	Orbit	Signal	R^2 (σ^0)	R^2 ($\Sigma\sigma^0$)
BBCH	168	σ^0_{VH}	0.46	0.97
Leaf number	73	$\sigma^0_{VH/VV}$	0.37	0.90
LAI	73	σ^0_{VH}	0.83	0.94
DMY	73	$\sigma^0_{VH/VV}$	0.39	0.93
DMC	73	$\sigma^0_{VH/VV}$	0.27	0.83

Notes: σ^0 indicates non time-integrated values of the backscattering coefficient, while $\Sigma\sigma^0$ indicates time-integrated values of the backscattering coefficient.

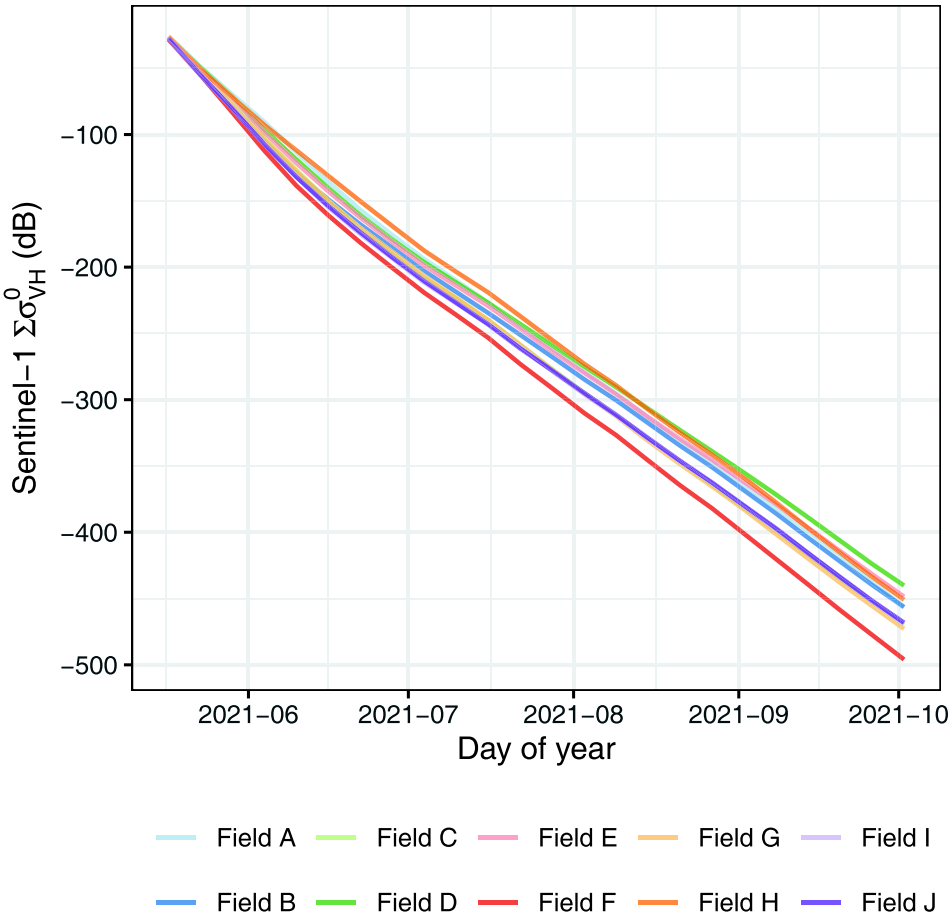

Figure 9. Time-integrated values of σ^0_{VH} for ten forage maize fields grown in 2021 and randomly selected within a 10 km radius of our field experiment.

The results presented in this study were obtained from measurements on a single site and year, which is insufficient to formally draw general conclusions on the robustness and accuracies of the models. The topography of the fields was flat, reducing risks of geometry effects on the backscattering coefficient. Moreover, the experiment was designed to minimise any stress, such as water or nitrogen deficit, or diseases. As a result, the growth and development of monitored maize fields is mostly time-dependent, and simple DAS-based model showed similarly good performances when used to estimate maize traits. However, in the case of real farming fields, stresses such as the ones mentioned above would occur, which could not be captured by simple DAS-based models.

In order to assess the capability of our approach to capture time-independent patterns, we computed the values of $\Sigma\sigma^0_{VH}$ for ten randomly selected silage maize fields grown in 2021 and located within a 10 km radius of our field experiment. The field geometries were obtained from the Land Parcel Identification System (LPIS), which is available from the Swedish Board of Agriculture (Jordbruksverket 2026). Accumulation was set to start on the 14th of May and finish on the 5th of October. The results (Figure 9) show clear differences between fields, as illustrated e.g. with fields H and D, for which a shift could be observed around early August. Moreover, the values on the last day of accumulation show a difference of up to 13% (between field F and field D), which indicates different growth patterns despite the close geographic location. Our approach uses dynamics of the σ^0 signal, which is strongly dependent on the development, growth and overall status of the crop, enabling capture of differences between fields located close to each other.

Conclusions

The objective of this pilot study was to assess how time-integrated backscattering coefficients from Sentinel-1 could be used to monitor development and growth of forage maize. To this end, phenological stage,

number of leaves, leaf area index, dry matter yield and dry matter content were measured from a field experiment located in Sweden in 2021. Sentinel-1 data were obtained from Google Earth Engine and time-integrated values of σ^0 were computed from sowing of the field experiment until the last day of field measurement. Time-integrated-based models showed promising results, with R^2 of 0.97, 0.93, 0.94, 0.95 and 0.86 for phenological stage, leaf number, leaf area index, dry matter yield and dry matter content, respectively, and largely outperformed models based on non-cumulative σ^0. Although no other study has reported the use of time-integrated backscattering coefficients for maize, our results are consistent with those obtained for rapeseed and winter wheat. This suggests that the time-integrated σ^0 approach is suitable for dense canopy and high biomass level crops such as maize or sugarcane. Importantly, the accuracy of regression models did not change when reducing the number of Sentinel-1 images to single orbit acquisitions, suggesting that the approach performs equally well with data acquired from a single Sentinel-1 satellite, and that the loss of a Sentinel-1 satellite should not affect the quality of the models. In addition, the recent launch of Sentinel-1 C should secure data acquisition in the coming years. With climate change, maize cultivation is expected to shift towards higher latitudes, including Nordic regions where frequent cloud cover can hinder optical remote sensing. Our approach could therefore be particularly valuable for monitoring maize and other crops in these areas. These preliminary results need to be confirmed by further studies that cover longer time periods, more locations, and a wider range of soil types, topography, and maize management practices. However, they suggest that a Sentinel-1 time-integrated approach could be useful to create a crop monitoring and decision support tool that works reliably regardless of weather conditions.

Acknowledgments

Maize seeds were graciously provided by KWS Scandinavia. The authors are grateful to field operators of Hushållningssällskapet Skåne, who performed field management and measurements.

Author contributions

CRediT: **Julien Morel:** Conceptualization, Data curation, Formal analysis, Funding acquisition, Writing – original draft, Writing – review & editing; **Frédéric Baup:** Conceptualization, Data curation, Formal analysis, Writing – review & editing; **Johan E. S. Fransson:** Conceptualization, Formal analysis, Writing – review & editing; **Mats Söderström:** Conceptualization, Formal analysis, Writing – review & editing; **David Parsons:** Conceptualization, Funding acquisition, Writing – review & editing; **Mårten Hetta:** Conceptualization, Funding acquisition, Writing – review & editing; **Susan Steele-Dunne:** Formal analysis, Writing – review & editing.

Data availability statement

Authors agree to make data and materials supporting the results or analyses presented in their paper available upon reasonable request. It is up to the author to determine whether a request is reasonable.

Disclosure statement

No potential conflict of interest was reported by the author(s).

Funding

This study was funded by the Lantmännen Research Foundation, Grant 2020H043.

ORCID

Julien Morel http://orcid.org/0000-0003-3209-5668
Frédéric Baup http://orcid.org/0000-0002-8824-9323
Johan E. S. Fransson http://orcid.org/0000-0002-7913-8592
Mats Söderström http://orcid.org/0000-0001-9946-0979
David Parsons http://orcid.org/0000-0002-1393-8431

Mårten Hetta http://orcid.org/0000-0002-8396-9786
Susan Steele-Dunne http://orcid.org/0000-0002-8644-3077

References

Allies A, et al. 2021. Evaluation of multiorbital SAR and multisensor optical data for empirical estimation of rapeseed biophysical parameters. IEEE J Sel Top Appl Earth Obs Remote Sens. 14:7268–7283. https://doi.org/10.1109/JSTARS.2021.3095537

Ameline M, Fieuzal R, Betbeder J, Berthoumieu JF, Baup F. 2018. Estimation of corn yield by assimilating SAR and optical time series into a simplified agro-meteorological model: from diagnostic to forecast. IEEE J Sel Top Appl Earth Obs Remote Sens. 11(12):4747–4760. https://doi.org/10.1109/JSTARS.2018.2878502

Battude M, et al. 2016. Estimating maize biomass and yield over large areas using high spatial and temporal resolution Sentinel-2 like remote sensing data. Remote Sens Environ. 184:668–681. https://doi.org/10.1016/j.rse.2016.07.030

Baup F, et al. 2019. Temporal evolution of corn mass production based on agro-Meteorological modelling controlled by satellite optical and SAR images. Remote Sens (Basel). 11(17):1978. https://doi.org/10.3390/rs11171978

Baup F, et al. 2026. 6 years of SAR (Sentinel-1) and optical (Sentinel 2, landsat-8) acquisitions over agricultural surfaces in southwestern France. Remote Sens (Basel). 18(5):790. https://doi.org/10.3390/rs18050790

Bazzi H, et al. 2020. Irrigation events detection over intensively irrigated grassland plots using Sentinel-1 data. Remote Sens (Basel). 12(24):4058. https://doi.org/10.3390/rs12244058

Bégué A, et al. 2018. Remote sensing and cropping practices: a review. Remote Sens (Basel). 10(1):99. https://doi.org/10.3390/rs10010099

Belward AS, Skøien JO. 2015. Who launched what, when and why; trends in global land-cover observation capacity from civilian earth observation satellites. ISPRS J Photogramm Remote Sens. 103:115–128. https://doi.org/10.1016/j.isprsjprs.2014.03.009

Campoy J, et al. 2023. Remote sensing-based crop yield model at field and within-field scales in wheat and barley crops. Eur J Agron. 143:126720. https://doi.org/10.1016/j.eja.2022.126720

Claverie M, et al. 2012. Maize and sunflower biomass estimation in southwest France using high spatial and temporal resolution remote sensing data. Remote Sens Environ. 124:844–857. https://doi.org/10.1016/j.rse.2012.04.005

den Besten N, et al. 2023. Understanding Sentinel-1 backscatter response to sugarcane yield variability and waterlogging. Remote Sens Environ. 290:113555. https://doi.org/10.1016/j.rse.2023.113555

Di Martino T, Guinvarc'h R, Thirion-Lefevre L, Koeniguer EC. 2022. Beets or cotton? Blind extraction of fine agricultural classes using a convolutional autoencoder applied to temporal SAR signatures. IEEE Trans Geosci Remote Sens. 60:1–18. https://doi.org/10.1109/TGRS.2021.3100637

d'Andrimont R, et al. 2020. Detecting flowering phenology in oil seed rape parcels with Sentinel-1 and -2 time series. Remote Sens Environ. 239:111660. https://doi.org/10.1016/j.rse.2020.111660

d'Andrimont R, et al. 2021. From parcel to continental scale – a first European crop type map based on Sentinel-1 and LUCAS Copernicus in-situ observations. Remote Sens Environ. 266:112708. https://doi.org/10.1016/j.rse.2021.112708

Fritz S, et al. 2019. A comparison of global agricultural monitoring systems and current gaps. Agric Syst. 168:258–272. https://doi.org/10.1016/j.agsy.2018.05.010

Gómez C, White JC, Wulder MA. 2016. Optical remotely sensed time series data for land cover classification: a review. ISPRS J Photogramm Remote Sens. 116:55–72. https://doi.org/10.1016/j.isprsjprs.2016.03.008

Gorelick N, et al. 2017. Google earth engine: planetary-scale geospatial analysis for everyone. Remote Sens Environ. 202:18–27. https://doi.org/10.1016/j.rse.2017.06.031

Gorrab A, Ameline M, Albergel C, Baup F. 2021. Use of Sentinel-1 multi-configuration and multi-temporal series for monitoring parameters of winter wheat. Remote Sens (Basel). 13(4):553. https://doi.org/10.3390/rs13040553

Hetta M, Mussadiq Z, Gustavsson AM, Swensson C. 2012. Effects of hybrid and maturity on performance and nutritive characteristics of forage maize at high latitudes, estimated using the gas production technique. Animal Feed Science and Technology. 171(1):20–30. https://doi.org/10.1016/j.anifeedsci.2011.09.015

Hird JN, McDermid GJ. 2009. Noise reduction of NDVI time series: an empirical comparison of selected techniques. Remote Sens Environ. 113(1):248–258. https://doi.org/10.1016/j.rse.2008.09.003

Jordbruksverket. 2026. Kartor och geografisk data. https://jordbruksverket.se/e-tjanster-databaser-och-appar/e-tjanster-och-databaser-stod/kartor-och-gis.

Kalogeropoulos G, Elli EF, Trifunovic S, Archontoulis SV. 2024. Historical increases of maize leaf area index in the US Corn Belt due primarily to plant density increases. Field Crops Res. 318:109615. https://doi.org/10.1016/j.fcr.2024.109615

Khabbazan S, et al. 2019. Crop monitoring using Sentinel-1 data: a case study from the Netherlands. Remote Sens (Basel). 11(16):1887. https://doi.org/10.3390/rs11161887

Kooistra L, et al. 2024. Reviews and syntheses: remotely sensed optical time series for monitoring vegetation productivity. Biogeosciences. 21(2):473–511. https://doi.org/10.5194/bg-21-473-2024

Lancashire PD, et al. 1991. A uniform decimal code for growth stages of crops and weeds. Ann Appl Biol. 119(3):561–601. https://doi.org/10.1111/j.1744-7348.1991.tb04895.x

Mandal D, et al. 2020. Dual polarimetric radar vegetation index for crop growth monitoring using sentinel-1 SAR data. Remote Sens Environ. 247:111954. https://doi.org/10.1016/j.rse.2020.111954
Meroni M, et al. 2021. Comparing land surface phenology of major European crops as derived from SAR and multispectral data of Sentinel-1 and -2. Remote Sens Environ. 253:112232. https://doi.org/10.1016/j.rse.2020.112232
Morel J, et al. 2014. Coupling a sugarcane crop model with the remotely sensed time series of fIPAR to optimise the yield estimation. Eur J Agron. 61:60–68. https://doi.org/10.1016/j.eja.2014.08.004
Planque C, et al. 2021. National crop mapping using sentinel-1 time series: a knowledge-based descriptive algorithm. Remote Sens (Basel). 13(5):846. https://doi.org/10.3390/rs13050846
Qadir A, Skakun S, Eun J, Prashnani M, Shumilo L. 2023. Sentinel-1 time series data for sunflower (Helianthus annuus) phenology monitoring. Remote Sens Environ. 295:113689. https://doi.org/10.1016/j.rse.2023.113689
Quast R, Wagner W, Bauer-Marschallinger B, Vreugdenhil M. 2023. Soil moisture retrieval from Sentinel-1 using a first-order radiative transfer model–a case-study over the Po-Valley. Remote Sens Environ. 295:113651. https://doi.org/10.1016/j.rse.2023.113651
Schmidt T, et al. 2024. Comprehensive quality assessment of satellite- and model-based soil moisture products against the COSMOS network in Germany. Remote Sens Environ. 301:113930. https://doi.org/10.1016/j.rse.2023.113930
Shammi SA, Meng Q. 2021. Use time series NDVI and EVI to develop dynamic crop growth metrics for yield modeling. Ecol Indic. 121:107124. https://doi.org/10.1016/j.ecolind.2020.107124
Shorachi M, Kumar V, Steele-Dunne SC. 2022. Sentinel-1 SAR backscatter response to agricultural drought in the Netherlands. Remote Sens (Basel). 14(10):2435. https://doi.org/10.3390/rs14102435
Steele-Dunne SC, et al. 2017. Radar remote sensing of agricultural canopies: a review. IEEE J Sel Top Appl Earth Obs Remote Sens. 10(5):2249–2273. https://doi.org/10.1109/JSTARS.2016.2639043
Torres R, et al. 2012. GMES sentinel-1 mission. Remote Sens Environ. 120:9–24. https://doi.org/10.1016/j.rse.2011.05.028
Veloso A, et al. 2017. Understanding the temporal behavior of crops using Sentinel-1 and Sentinel-2-like data for agricultural applications. Remote Sens Environ. 199:415–426. https://doi.org/10.1016/j.rse.2017.07.015
Weiss M, Jacob F, Duveiller G. 2020. Remote sensing for agricultural applications: a meta-review. Remote Sens Environ. 236:111402. https://doi.org/10.1016/j.rse.2019.111402
Wiseman G, McNairn H, Homayouni S, Shang J. 2014. RADARSAT-2 polarimetric SAR response to crop biomass for agricultural production monitoring. IEEE J Sel Top Appl Earth Obs Remote Sens. 7(11):4461–4471. https://doi.org/10.1109/JSTARS.2014.2322311
Zscheischler J, et al. 1990. Handbuch Mais: umweltgerechter Anbau, wirtschaftliche Verwertung. 4., vollkommen überarbeitete auflage ed. DLG-Verlag. ISBN 978-3-7690-0473-1. OCLC: 230999125.

Appendices

Appendix 1. Leave-one-out cross validation vs. using all data

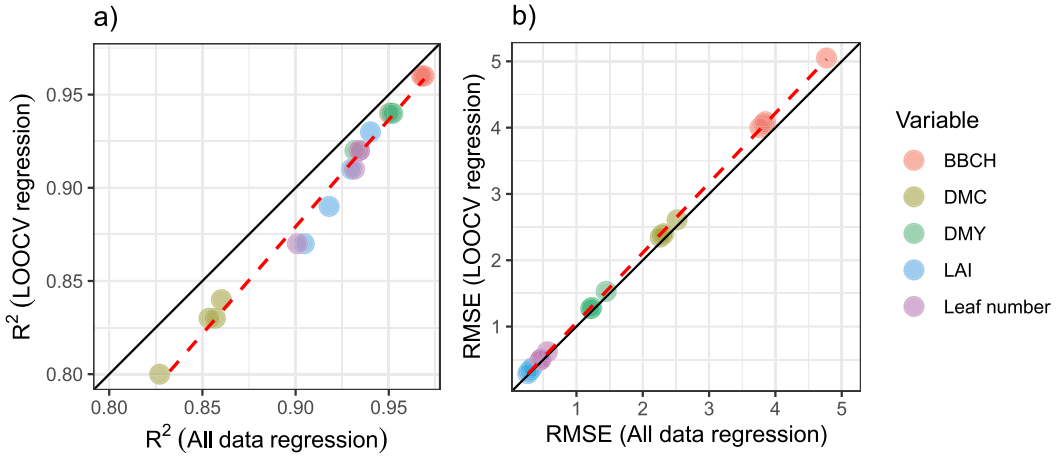

Figure A1. Comparison of R^2 and *RMSE* for models built with all available data and using a leave-one-out cross-validation approach. Red dashed lines indicate the regression line and grey lines indicate the 1:1 line.

Figure A1 compares R^2 and *RMSE* obtained from models built using all available data and a leave-one-out cross-validation approach for the mixed orbit signal approach. R^2 and *RMSE* from both approaches show good agreement, suggesting that using all data for building our models did not lead to biased performances.

Appendix 2. Linear regression coefficients

Table A1 provides the regression coefficients of the models built using all available data for the mixed orbit signal approach.

Table A1. Regression coefficients of the models.

Variable	$\Sigma\sigma^0$	Linear regression		Logistic regression		
		a	*b*	*m*	*c*	x_i
BBCH	σ^0_{VH}	N/A	N/A	78.9	−151.2	−839.9
BBCH	$\sigma^0_{VH/VV}$	N/A	N/A	79.3	−59.7	−337.0
BBCH	$\sigma^0_{VH\times VV}$	N/A	N/A	78.9	−244.0	−1343.0
BBCH	σ^0_{VV}	N/A	N/A	78.9	−93.3	−503.0
Leaf number	σ^0_{VH}	−0.01	−2.4	N/A	N/A	N/A
Leaf number	$\sigma^0_{VH/VV}$	−0.03	−1.8	N/A	N/A	N/A
Leaf number	$\sigma^0_{VH\times VV}$	−0.01	−2.4	N/A	N/A	N/A
Leaf number	σ^0_{VV}	−0.02	−2.3	N/A	N/A	N/A
Leaf number*	σ^0_{VH}	0.002	14.2	N/A	N/A	N/A
Leaf number*	$\sigma^0_{VH/VV}$	0.006	14.2	N/A	N/A	N/A
Leaf number*	$\sigma^0_{VH\times VV}$	0.001	14.2	N/A	N/A	N/A
Leaf number*	σ^0_{VV}	0.004	14.1	N/A	N/A	N/A
LAI	σ^0_{VH}	N/A	N/A	3.2	−32.5	−753.4
LAI	$\sigma^0_{VH/VV}$	N/A	N/A	3.2	−14.8	−301.2
LAI	$\sigma^0_{VH\times VV}$	N/A	N/A	3.2	−53.9	−1200.3
LAI	σ^0_{VV}	N/A	N/A	3.2	−20.2	−447.0
DMY	σ^0_{VH}	−0.02	−10.5	N/A	N/A	N/A
DMY	$\sigma^0_{VH/VV}$	−0.05	−11.2	N/A	N/A	N/A
DMY	$\sigma^0_{VH\times VV}$	0.01	−10.3	N/A	N/A	N/A
DMY	σ^0_{VV}	−0.03	−9.9	N/A	N/A	N/A
DMC	σ^0_{VH}	−0.02	−0.9	N/A	N/A	N/A
DMC	$\sigma^0_{VH/VV}$	−0.05	−1.5	N/A	N/A	N/A
DMC	$\sigma^0_{VH\times VV}$	−0.01	−0.7	N/A	N/A	N/A
DMC	σ^0_{VV}	−0.03	−0.3	N/A	N/A	N/A

Notes: *a* and *b* are the slope and intercept of the linear models; *m*, *c* and x_i are respectively the maximum σ^0 of the logistic curve, the slope at the inflexion point of the function and the time-integrated σ^0 at the inflexion point *i*. 'Leaf number' indicates models built for the vegetative phase of maize, while 'Leaf number*' indicates models built for the maturity phase of maize. N/A indicates non relevant values.